ESMO GOOD SCIENCE BETTER MEDICINE BEST PRACTICE

ESMO OPEN SCIENCE FOR OPTIMAL CANCER CARE

ORIGINAL ARTICLE

Integrating radiomics, pathomics, and biopsy-adapted immunoscore for predicting distant metastasis in locally advanced rectal cancer

R. Zhao[1†], W. Shen[2†], W. Zhao[3,4,5†], W. Peng[1†], L. Wan[1], S. Chen[1], X. Liu[1], S. Wang[6], S. Zou[2*], R. Zhang[1*] & H. Zhang[1*]

Departments of [1]Diagnositic Radiology; [2]Pathology, National Cancer Center/National Clinical Research Center for Cancer/Cancer Hospital, Chinese Academy of Medical Sciences and Peking Union Medical College, Beijing; [3]Department of Colorectal Surgery, Tianjin Union Medical Center, Tianjin; [4]The Institute of Translational Medicine, Tianjin Union Medical Center, Nankai University, Tianjin; [5]Tianjin Institute of Coloproctology, Tianjin; [6]Department of Pharmaceutical Diagnosis, GE Healthcare, Life Sciences, Beijing, China

Available online xxx

Background: This study aimed to develop and validate a nomogram that utilized macro- and microscopic tumor characteristics at baseline, including radiomics, pathomics, and biopsy-adapted immunoscore (IS_B), to accurately predict distant metastasis (DM) in patients with locally advanced rectal cancer (LARC) who underwent neoadjuvant chemoradiotherapy (nCRT).

Materials and methods: In total, 201 patients with LARC (91 months of median follow-up) were enrolled. Radiomics features were extracted from apparent diffusion coefficient maps and T2-weighted images. Pathomics features including global pattern (features of the entire image) and local pattern (features of the tumor nuclei) were extracted from whole-slide images of hematoxylin—eosin-stained biopsy specimens. IS_B was calculated from the densities of CD3+ and CD8+ T cells in the tumor region using immunohistochemistry on biopsy specimens. The construction of a predictive model was carried out using the least absolute shrinkage and selection operator-Cox analysis, with performance metrics including the area under the curve (AUC) and concordance index (C-index) utilized for evaluation.

Results: Compared with patients with moderate and high IS_B, patients with low IS_B exhibited significantly higher risk scores for radiomics and pathomics signatures. The nomogram showed respective C-indexes of 0.902 and 0.848 for 5-year DM-free survival in the training and test sets, along with corresponding AUC values of 0.950 and 0.872. Patients could be efficiently categorized into low- and high-risk groups for developing DM using the nomogram.

Conclusions: The nomogram integrating macroscopic radiological information and microscopic pathological information is effective for risk stratification at baseline in LARC treated with nCRT.

Key words: rectal cancer, distant metastasis, radiomics, pathomics, immunoscore

*Correspondence to: Prof. Hongmei Zhang, Department of Diagnostic Radiology, National Cancer Center/National Clinical Research Center for Cancer/Cancer Hospital, Chinese Academy of Medical Sciences and Peking Union Medical College, #17 Panjiayuan Nanli, Chaoyang District, Beijing, 100021, China. Tel: +8613581968865

E-mail: 13581968865@163.com (H. Zhang).

Prof. Renzhi Zhang, Department of Diagnostic Radiology, National Cancer Center/National Clinical Research Center for Cancer/Cancer Hospital, Chinese Academy of Medical Sciences and Peking Union Medical College, #17 Panjiayuan Nanli, Chaoyang District, Beijing, 100021, China. Tel: +8613718139121

E-mail: zhangrenzhi7790@126.com (R. Zhang).

Prof. Shuangmei Zou, Department of Pathology, National Cancer Center/National Clinical Research Center for Cancer/Cancer Hospital, Chinese Academy of Medical Sciences and Peking Union Medical College, #17 Panjiayuan Nanli, Chaoyang District, Beijing, 100021, China. Tel: +8613681079941

E-mail: smzou@hotmail.com (S. Zou).

†These authors contributed equally to the work.

INTRODUCTION

The current standard treatment for locally advanced rectal cancer (LARC; T3-4 and/or N1-2, M0) is neoadjuvant chemoradiotherapy (nCRT) followed by total mesorectal excision. Despite reducing the local recurrence rate to 5%-10%,[1,2] there has been limited progress in significantly improving the occurrence of distant metastasis (DM). DM remains the leading cause of mortality for LARC patients, with a prevalence of 25%-40%.[3,4] nCRT followed by surgery inevitably delayed the delivery of systemic treatment. Adjuvant chemotherapy as the systemic treatment after the standard treatment is still controversial owing to poor compliance and uncertain survival benefits.[5-7] The situation highlights the necessity of making upfront treatment strategies, including earlier systemic treatment before surgery,

to control underlying micro-metastasis. Therefore, a risk stratification model that provides prognostic information before treatment would be useful for optimizing treatment and surveillance.

High-throughput omics, including radiomics and pathomics, are the computational analysis of medical images to extract numerous quantitative imaging features that are visually challenging to detect. This approach could explore the underlying associations between the features and tumor biological behaviors.[8] Magnetic resonance imaging (MRI) is an important component of staging and treatment planning for rectal cancer. Previous studies suggested that radiomics derived from MRI could potentially forecast prognosis for patients with rectal cancer.[9,10] Pathological evaluation of endoscopic biopsy specimens serves as the gold standard for diagnosing rectal cancer. Pathomics features, obtained by machine learning from hematoxylin–eosin (H&E)-stained biopsy slides, contain subvisual morphometric phenotypes that offer microstructural information about the tumor microenvironment.[11,12] Two recent studies on patients with LARC have provided evidence that pathomics could predict treatment response to nCRT.[13,14] In addition, previous studies have highlighted that the *in situ* immune cell infiltrate deeply influences the patient prognosis.[15,16] In rectal cancer, the natural immune reaction of the tumor has been shown to be evaluated on biopsies.[17-19] Biopsy-adapted immunoscore (IS_B) derived from the calculation of the densities of CD3+ and CD8+ T cells through immunohistochemistry in biopsy specimens is a highly reliable biomarker for estimating the treatment response to nCRT and prognosis.[20]

To our knowledge, research is lacking on the use of integrating radiological information at the macroscale and pathological information at the microscale to predict survival outcomes in LARC. The study integrated radiomics, pathomics, and IS_B to enrich tumor descriptors and construct a powerful model for the prediction of DM-free survival in LARC treated with nCRT.

MATERIALS AND METHODS

Patients

Our institution's ethics committee approved this study, and because it was retrospective in nature, informed consent was waived. Three hundred and twenty-seven consecutive patients with a confirmed diagnosis of LARC (T3-4 and/or N1-2, M0) who underwent rectal MRI within 2 weeks before therapy were included in the study, which was carried out from June 2011 to June 2017. Patients were excluded if: (i) they had mucinous adenocarcinoma (due to distinctive signal on T2-weighted images) ($n = 28$), (ii) they had a history of other primary malignant tumors ($n = 32$), (iii) they were lost to follow-up ($n = 31$), (iv) they had low-quality MRI images ($n = 6$), and (v) they lacked pathological biopsy slides ($n = 29$). Finally, 201 patients were analyzed (7 : 3 randomization between the training and test groups). Baseline clinical characteristics are summarized in Supplementary Table S1, available at https://doi.org/10.1016/j.esmoop.2024.104102. The whole pipeline is illustrated in Figure 1.

MRI examination

A 3.0-T MRI system (Discovery MR 750; General Electrics, Waukesha, WI) was used for all MRI examinations. The imaging protocols included axial T1-weighted imaging, oblique axial T2-weighted imaging (T2WI), coronal T2WI, sagittal T2WI, and axial diffusion-weighted imaging (with b values of 0 and 800 s/mm^2). Automatically generated apparent diffusion coefficient (ADC) maps were constructed using a monoexponential decay model that incorporated both b values. Protocols for the MRI sequence are summarized in Supplementary Table S2, available at https://doi.org/10.1016/j.esmoop.2024.104102.

Treatment

The regimen of nCRT included radiotherapy (45-50.4 Gy) administered in 25 fractions of 1.8-2 Gy, along with concurrent chemotherapy (capecitabine 1650 mg/m^2, orally). After surgery, adjuvant therapy was administered to patients with high-risk factors as determined by oncologists.

Follow-up

Regular follow-up assessments were conducted with all patients. Visits were conducted every 3 months for the initial 2-year period, followed by visits every 6 months for the subsequent 3-year period. Afterward, visits were conducted annually. DM was defined as recurrence in other organs/sites (including liver, lung, bone, and non-regional lymph nodes) or peritoneal metastasis, which was determined using imaging and/or biopsy. DM-free survival was defined as the interval time between the surgery and the occurrence of DM. Patients were considered censored if they had no DM during the follow-up period. The final follow-up for this study was conducted in March 2023.

Radiomics feature extraction

Volumes of interest (VOIs) encompassing the entire rectal tumor were manually delineated on oblique axial T2-weighted images and ADC maps using ITK-SNAP software (version 3.8.0, http://www.itksnap.org) by a board-certified radiologist with 6 years' experience in gastrointestinal imaging. Subsequently, all VOIs were thoroughly reviewed by a senior radiologist with 23 years' experience in gastrointestinal imaging. Two radiologists resolved any disputes through consensus. Then, a board-certified radiologist with 7 years' experience in gastrointestinal imaging segmented 30 randomly selected rectal tumors again in order to mitigate the potential negative impact on the extracted features resulting from manual segmentation. All radiologists were blinded to the patient data during the segmentation process. Utilizing the intraclass correlation coefficient (ICC), the interobserver reproducibility of feature extraction was assessed. Relevant radiomics features, demonstrating satisfactory reproducibility with an ICC value exceeding

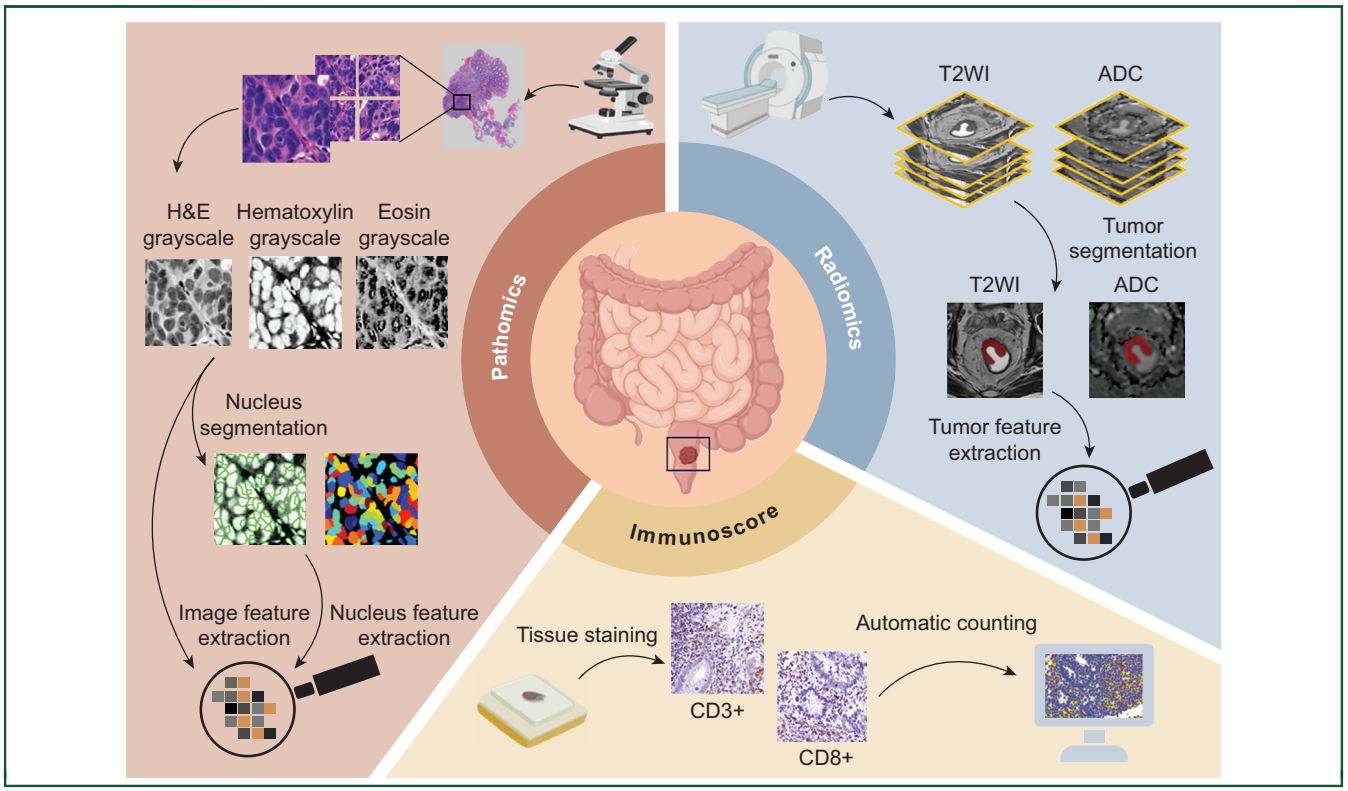

Figure 1. Schematic of the study pipeline.
ADC, apparent diffusion coefficient; H&E, hematoxylin–eosin; T2WI, T2-weighted imaging.

0.75, were chosen for subsequent analysis. Preprocessing of images and extraction of radiomics features were conducted on the Radcloud platform, utilizing the 'pyradiomics' module in Python 3.8.1 (https://pyradiomics.readthedocs.io/). A total of 2074 radiomics features were extracted, comprising 1037 radiomics features from T2-weighted images and 1037 radiomics features from ADC maps. Supplementary Methods, available at https://doi.org/10.1016/j.esmoop.2024.104102, contain further details about radiomics feature extraction. Supplementary Table S3, available at https://doi.org/10.1016/j.esmoop.2024.104102, provides a summary of the radiomics features.

Pathomics feature extraction

Formalin-fixed paraffin-embedded samples were utilized in the preparation of biopsy specimen slides stained with H&E. Next, all H&E-stained slides were scanned by a pathologist with 2 years' experience in pathological diagnosis using a scanner (KF-PRO-040, KFBIO, Ningbo, Zhejiang, China) to obtain whole-slide images (WSIs). Subsequently, the board-certified pathologist selected 10 nonoverlapping representative tiles from each WSI, containing the greatest number of tumor cells in a field of view of 1000 × 1000 pixels at ×20 magnification (0.5 μm/pixel). The selected tiles were confirmed by a senior pathologist with 22 years' experience in pathological diagnosis. The CellProfiler software (version 4.2.5, https://cellprofiler.org) was used to extract the pathomics features. Six hundred and twenty-one pathomics features were extracted and are summarized in Supplementary Table S4, available at https://doi.org/10.1016/j.esmoop.2024.104102. Supplementary Methods, available at https://doi.org/10.1016/j.esmoop.2024.104102, contain more information about the extraction of pathomics features.

Signature construction

Standardization of extracted radiomics and pathomics features was carried out using z-scores. The training dataset was utilized to carry out the feature selection. At first, univariate Cox analysis was implemented to identify features with a P value <0.1 for subsequent analysis. Then, Spearman correlation coefficients (ρ) were computed for each pair of features. Pairs of features with $|\rho| > 0.8$ were recognized, and only the feature with the greater mean absolute correlation was retained, while the other one was excluded. Subsequently, a least absolute shrinkage and selection operator (LASSO)-Cox analysis, incorporating 10-fold cross-validation, was implemented separately for the identification of the most powerful radiomics and pathomics features. Finally, radiomics and pathomics

signatures were generated using the most valuable radiomics and pathomics features, respectively.

Biopsy-adapted immunoscore determination

The process of immunohistochemistry staining is described in the Supplementary Methods, available at https://doi.org/10.1016/j.esmoop.2024.104102. The densities of CD3+ and CD8+ T cells in the tumor region were assessed with the HALO Highplex FL module of the HALO Image analysis platform (Indica Labs, Albuquerque, NM). Determination of IS_B established by El Sissy et al.[20] was derived from the methodology to determine the Immunoscore® (IS).[21] The densities of CD3+ and CD8+ T cells in the tumor region for individual patients were compared with those obtained from all patients and transformed into percentiles. Subsequently, the mean of the two percentiles (CD3+ and CD8+ T cells) was used to categorize patients into one of the three IS_B groups: low (<25%), intermediate (>25%-70%), and high (>70%-100%) (Supplementary Figure S1, available at https://doi.org/10.1016/j.esmoop.2024.104102).

Statistics analysis

Chi-square or Fisher's exact tests were used to compare the clinical variables in the training and test sets. The univariate and multivariate Cox analyses were employed to assess the radiomics signature, pathomics signature, IS_B, and clinical variables, with the goal of identifying independent predictors for DM-free survival and constructing a predictive nomogram within the training set. The nomogram's performance was independently validated using the test set. The predictive performance was evaluated by the concordance index (C-index) and area under the curve (AUC) of the time-dependent receiver operating characteristic (ROC) curve.

The optimal cut-off value for the risk score of the nomogram was derived from the maximally selected rank statistics method to categorize individuals into low- and high-risk groups. Survival curves were created through Kaplan–Meier analysis, and statistical significance was assessed using the log-rank test.

The statistical analyses were carried out using R software (version 4.2.2, https://www.r-project.org). A P value <0.05 was considered statistically significant.

RESULTS

Patients

Overall, 201 participants (142 men and 59 women) were enrolled, with a mean age of 54.5 ± 10.6 years (range 23-79 years). In this study, R0 radical excision was carried out in all the cases. The median duration of follow-ups was 91 months (interquartile range 82-113 months). The 1-, 3-, and 5-year DM-free survival rates were 85.6%, 80.1%, and 75.6%, respectively. A 7 : 3 ratio was used to randomly divide the patients into two sets: a training set ($n = 140$) and a test set ($n = 61$). The training and the test sets had no statistically significant differences in clinical characteristics, including age, sex, carcinoembryonic antigen level, CA 19-9 level, tumor location, as well as clinical T and N stage (all, $P > 0.05$) (Table 1).

Signature construction

After implementing the interobserver assessment, 1328 radiomics features were left as stable features. To create the radiomics signature, seven radiomics features were incorporated through feature selection using LASSO-Cox analysis. The selected radiomics features are summarized in Supplementary Figure S2 and Table S5, available at https://doi.org/10.1016/j.esmoop.2024.104102. In terms of predicting DM-free survival, C-indexes of the radiomics signature achieved respective values of 0.811 [95% confidence interval (CI) 0.746-0.877] and 0.752 (95% CI 0.615-0.881) in the training and test sets.

Separately, through a feature selection using LASSO-Cox analysis, seven pathomics features were incorporated to create the pathomics signature. The selected pathomics features are summarized in Supplementary Figure S3 and Table S6, available at https://doi.org/10.1016/j.esmoop.2024.104102. In terms of predicting DM-free survival, C-indexes of the pathomics signature achieved respective values of 0.713 (95% CI 0.625-0.800) and 0.702 (95% CI 0.569-0.835) in the training and test sets.

Biopsy-adapted immunoscore

In the tumor region, the median density of CD3+ and CD8+ T cells was 681 cells/mm^2 and 436 cells/mm^2, respectively. In the training set, 22 (15.7%) patients had a low IS_B, 81 (57.9%) patients had an intermediate IS_B, and 37 (26.4%) patients had a high IS_B. Patients with low IS_B were more likely to develop DM than those with intermediate and high IS_B [intermediate versus low: hazard ratio (HR) 0.224, 95% CI 0.111-0.451, $P < 0.001$; high versus low: HR 0.080, 95% CI 0.023-0.276, $P < 0.001$]. Patients with intermediate IS_B were more likely to develop DM than those with high IS_B, but the difference was not statistically significant (HR 0.355, 95% CI 0.104-1.211, $P = 0.098$). Patients with low, intermediate, and high IS_B had 5-year DM-free survival rates of 36.4%, 79.0%, and 91.9%, respectively (Supplementary Figure S4A, available at https://doi.org/10.1016/j.esmoop.2024.104102).

Similar results were confirmed in the test set. In the test set, 10 (16.4%) patients had a low IS_B, 38 (62.3%) patients had an intermediate IS_B, and 13 (21.3%) patients had a high IS_B. Patients with low IS_B were more likely to develop DM than those with intermediate and high IS_B (intermediate versus low: HR 0.209, 95% CI 0.075-0.584, $P = 0.003$; high versus low: HR 0.068, 95% CI 0.008-0.562, $P = 0.013$). Patients with intermediate IS_B were more likely to develop DM than those with high IS_B, but the difference was not statistically significant (HR 0.326, 95% CI 0.041-2.611, $P = 0.291$). Patients with low, intermediate, and high IS_B had 5-year DM-free survival rates of 30.0%, 86.8%, and 92.3%, respectively (Supplementary Figure S4B, available at https://doi.org/10.1016/j.esmoop.2024.104102).

Table 1. Univariate and multivariate Cox regression analysis for distant metastasis (DM)-free survival

	Univariate Cox analysis		Multivariate Cox analysis	
	HR (95% CI)	*P* value	HR (95% CI)	*P* value
Age, years				
≥55 versus <55	1.418 (0.721-2.788)	0.312	NA	
Sex				
Male versus female	1.099 (0.538-2.244)	0.795	NA	
CEA level, ng/ml				
≥5 versus <5	1.293 (0.651-2.567)	0.462	NA	
CA 19-9 level, U/ml				
≥37 versus <37	2.044 (0.793-5.271)	0.139	NA	
Clinical T stage				
cT3b-T4 versus cT2-T3a	1.587 (0.693-3.633)	0.275	NA	
Clinical N stage				
cN1-2 versus cN0	2.235 (1.047-4.772)	0.038	2.322 (1.018-5.295)	0.045
Tumor location (cm)				
5-10 versus <5	0.622 (0.317-1.221)	0.168	NA	
>10 versus <5	0.243 (0.032-1.823)	0.169		
IS_B				
Intermediate versus low	0.224 (0.111-0.451)	<0.001	0.564 (0.263-1.208)	0.140
High versus low	0.080 (0.023-0.276)	<0.001	0.169 (0.048-0.598)	0.006
Radiomics signature	2.701 (1.963-3.716)	<0.001	2.538 (1.782-3.615)	<0.001
Pathomics signature	2.699 (1.781-4.090)	<0.001	1.983 (1.355-2.900)	<0.001

CA 19-9, carbohydrate antigen 19-9; CEA, carcinoembryonic antigen; CI, confidence interval; HR, hazard ratio; NA, not applicable.

Further, we characterized the distribution of the risk scores of radiomics and pathomics signatures among patients with different groups of IS_B and it suggested that patients with low IS_B have significantly higher risk scores of radiomics and pathomics signatures than those with intermediate and high IS_B in the training and test sets. Nevertheless, patients with intermediate and high IS_B did not differ statistically significantly in their risk scores for radiomics and pathomics signatures (Figure 2).

Nomogram

After conducting both univariate and multivariate Cox analyses, several independent factors were identified for the construction of the combined model. These factors included clinical N stage (cN1-2 versus cN0: HR 2.322, 95% CI 1.018-5.295, $P = 0.045$), IS_B (intermediate versus low: HR 0.564, 95% CI 0.263-1.208, $P = 0.140$; high versus low: HR 0.169, 95% CI 0.048-0.598, $P = 0.006$), radiomics signature (HR 2.538, 95% CI 1.782-3.615, $P < 0.001$), and pathomics signature (HR 1.983, 95% CI 1.355-2.900, $P < 0.001$) (Table 1). The combined model was visualized as a nomogram for ease of clinical use (Figure 3). The nomogram showed strong power in DM-free survival prediction, with respective C-indexes of 0.902 (95% CI 0.870-0.933) and 0.848 (95% CI 0.743-0.951) in the training and test sets. In the training set, the AUCs of the nomogram achieved 0.930 (95% CI 0.884-0.976), 0.947 (95% CI 0.910-0.983), and 0.950 (95% CI 0.916-0.985) in predicting 1-, 3-, and 5-year DM-free survival, respectively. In the test set, the AUCs of the nomogram achieved 0.940 (95% CI 0.858-1.000), 0.889 (95% CI 0.789-0.990), and 0.872 (95% CI 0.769-0.976) in predicting 1-, 3-, and 5-year DM-free survival, respectively (Figure 4A and B). Excellent agreement was observed between the actual status and the predicted outcomes of DM-free survival for patients with LARC using calibration curves of nomogram (Figure 4C and D). Nomogram performed better than radiomics signature, pathomics signature, and IS_B in predicting 1-, 3-, and 5-year DM-free survival in the training and test sets. AUCs, sensitivities, and specificities of time-dependent ROC curves in radiomics signature, pathomics signature, IS_B, and nomogram in the training and test sets are shown in Supplementary Tables S7 and S8, available at https://doi.org/10.1016/j.esmoop.2024.104102. The decision curves demonstrated the considerable net benefit of the nomogram in the training and test sets (Supplementary Figures S5A and S5B, respectively, available at https://doi.org/10.1016/j.esmoop.2024.104102).

Risk stratification

The formulas for the risk scores of radiomics signature, pathomics signature, and nomogram are shown in the Supplementary Note, available at https://doi.org/10.1016/j.esmoop.2024.104102. To categorize patients into low- and high-risk groups, a cut-off value of 0.188 was applied to the risk score of the nomogram. Thirty-eight patients (27.1%) and 13 patients (21.3%) with a risk score ≥0.188 were classified as high-risk group in the training and test sets. The high-risk group exhibited worse DM-free survival outcomes compared with the low-risk group in both the training (HR 25.168, 95% CI 10.332-61.368, $P < 0.001$, 5-year DM-free survival: 23.7% versus 95.1%) and test sets (HR 11.772, 95% CI 4.130-33.551, $P < 0.001$, 5-year DM-free survival: 23.1% versus 89.6%) (Figure 4E and F).

DISCUSSION

While the local recurrence rate could be reduced effectively with nCRT followed by surgery, the occurrence of DM remains a challenge. It is imperative to establish a risk

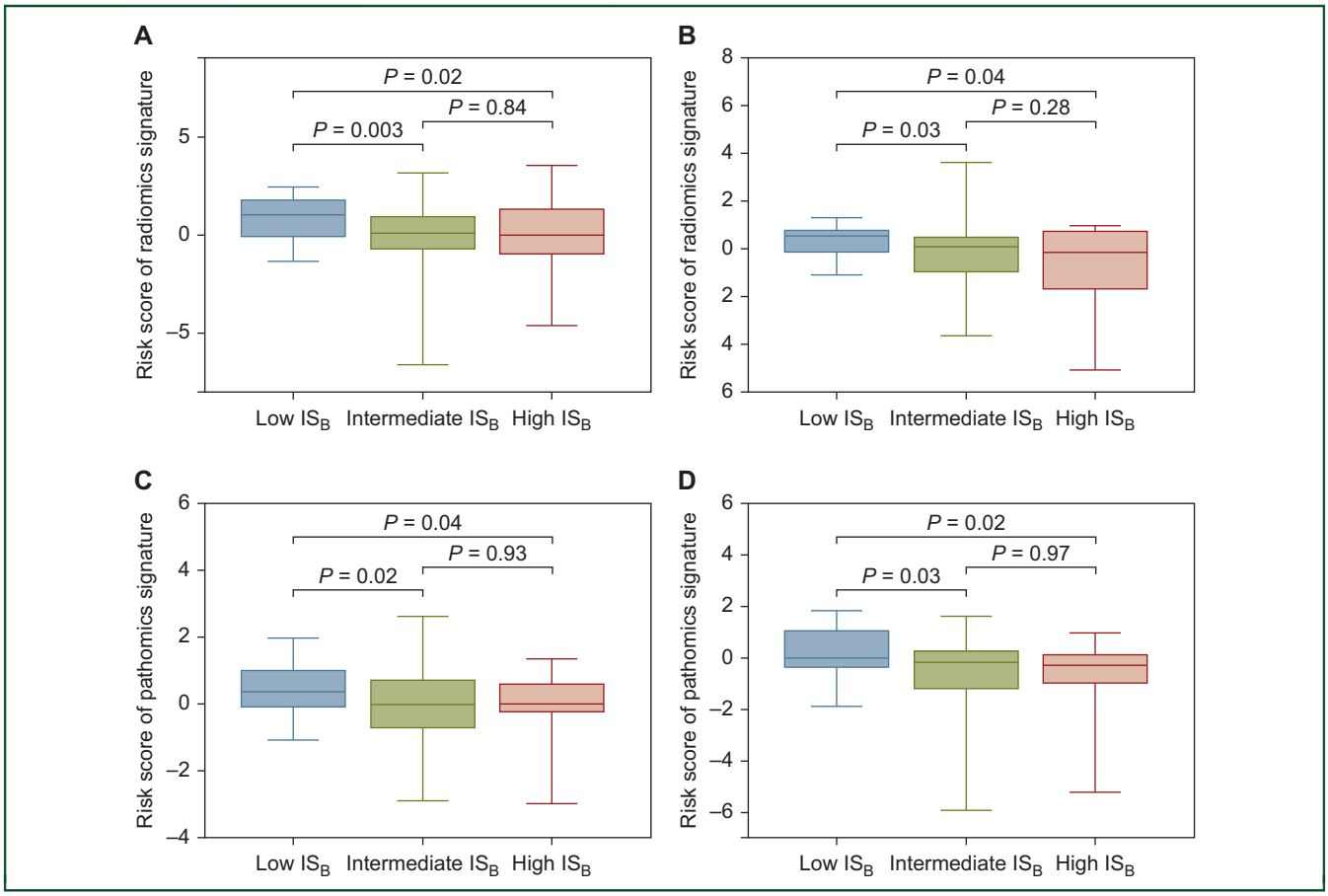

Figure 2. The correlation among the radiomics signature, pathomics signature, and biopsy-adapted immunoscore (IS_B). Comparison of the risk score of radiomics signature for distant metastasis (DM)-free survival among patients with low, intermediate, and high IS_B in the training (A) and test (B) sets. Comparison of the risk score of pathomics signature for DM-free survival among patients with low, intermediate, and high IS_B in the training (C) and test (D) sets.

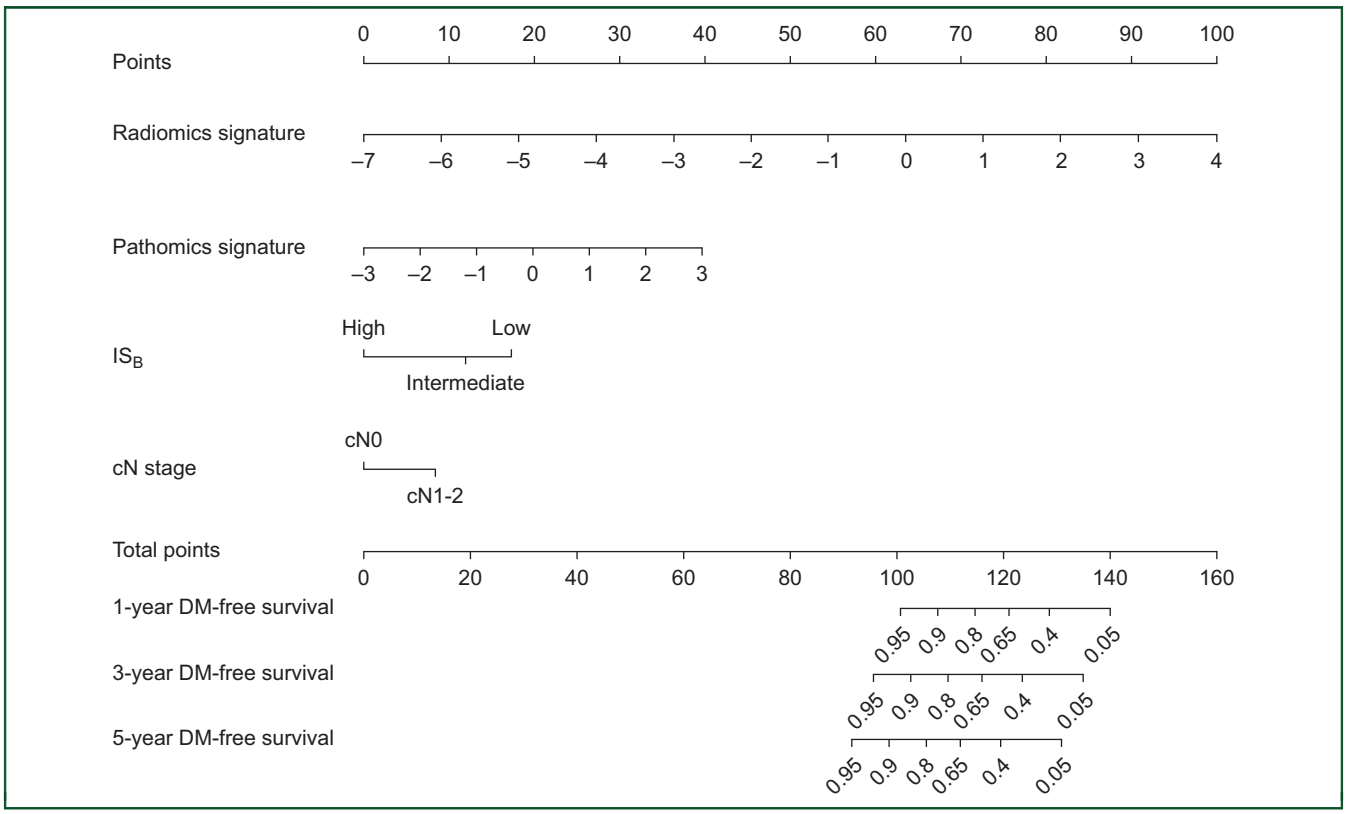

Figure 3. Nomogram for predicting 1-, 3-, and 5-year distant metastasis (DM)-free survival in locally advanced rectal cancer (LARC). IS_B, biopsy-adapted immunoscore.

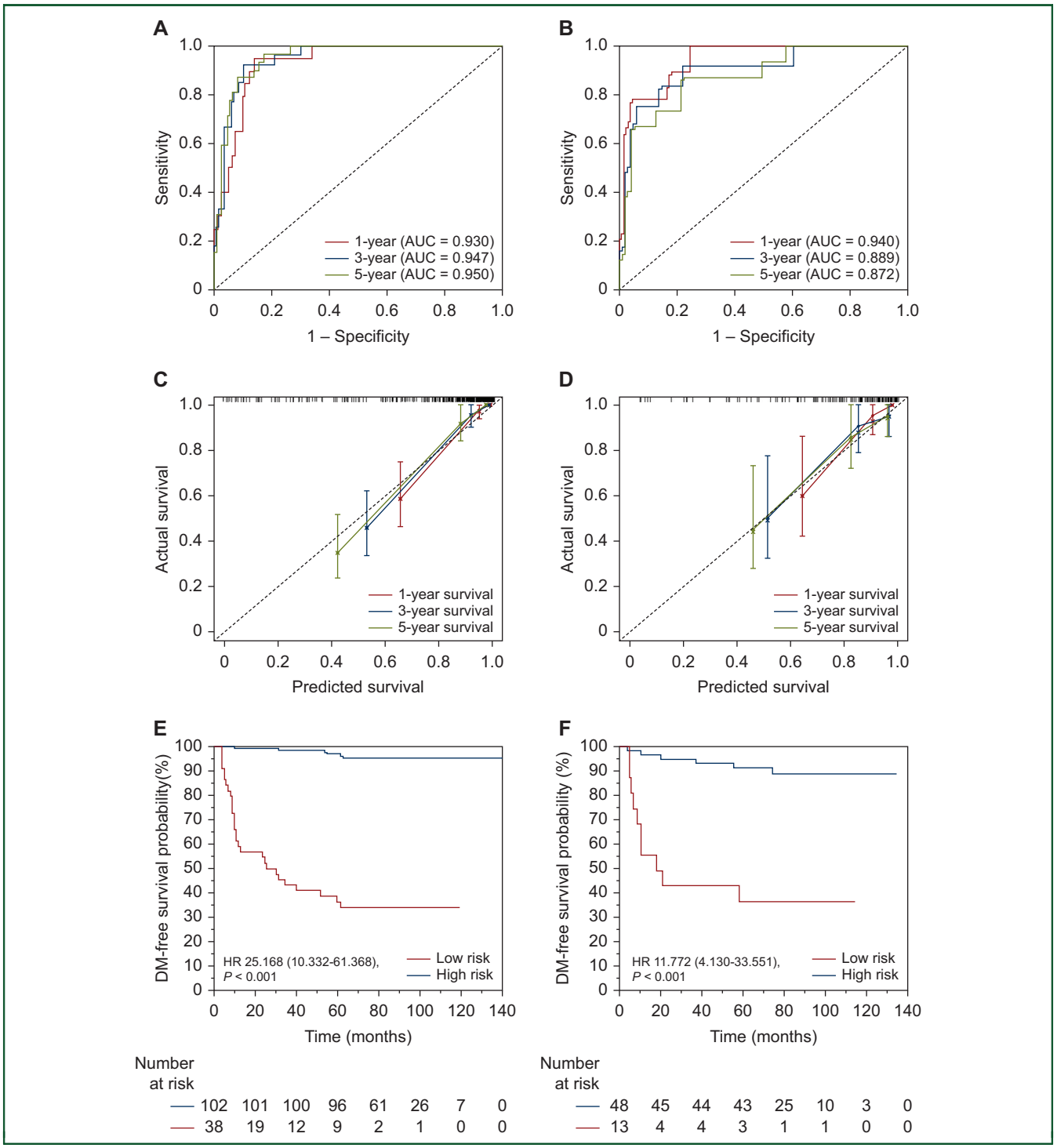

Figure 4. Predictive performance of the nomogram. Time-dependent receiver operating characteristic (ROC) curves of the nomogram for predicting 1-, 3-, and 5-year distant metastasis (DM)-free survival in the training (A) and test (B) sets. Calibration curves of the nomogram for predicting 1-, 3-, and 5-year DM-free survival in the training (C) and test (D) sets. Survival curves depicting DM-free survival for patients in the low- and high-risk groups in the training (E) and test (F) sets.
AUC, area under the curve; HR, hazard ratio.

stratification model for patients with LARC before treatment to identify high-risk patients with DM and develop a personalized neoadjuvant treatment. Tumors exhibit complex biological properties and interact with numerous factors, hence integrating multiscale information can enhance tumor characterization and facilitate the construction of a robust model.[22,23] This study built a nomogram integrating radiological information at the macroscale and pathological information at the microscale and demonstrated that the nomogram is highly effective in identifying high-risk patients with DM.

Radiomics can noninvasively capture tumor heterogeneity in voxels related to risk, identifying radiographic phenotypes and providing additional prognosis

https://doi.org/10.1016/j.esmoop.2024.104102

information. The potential of radiomics in guiding personalized treatment is widely recognized in rectal cancer.[24-26] Liu et al.[10] built a deep-learning radiomics signature using T2-weighted images and ADC maps, and also designed a nomogram that integrated the deep-learning radiomics signature with clinicopathological variables to predict DM following nCRT. The radiomics signature performed slightly better in our study than the deep-learning radiomics signature of Liu et al. (C-index of the test set: 0.752 versus 0.747). Furthermore, the nomogram established by Liu et al. necessitates reliance on the pathological factor, which can solely be acquired after surgical intervention and does not assist in the preoperative determinations.

While radiomics captures the spatial macrostructure of tumors, pathomics could provide in-depth microstructural information. Pathomics is a novel approach employed to investigate tumor heterogeneity, considering the correlation between a range of histologic features and varying degrees of clinical outcome.[27] Recent studies have shown that pathomics features extracted from WSIs of biopsy specimens can be utilized to predict the treatment response after nCRT.[13,14] At present, the literature on the analysis of DM among LARC patients has not been reported. In our study, pathomics features included both the local patterns (features of the tumor nucleus) and global patterns (features of the entire image) from WSI of H&E-stained slides. Yu et al.[28] demonstrated that the Zernike shape feature of the nuclei was the most important feature associated with the survival outcomes in non-small-cell lung cancer. Consistent with the previous study, we also discovered that the most important feature associated with DM for patients with LARC is the Zernike shape feature of the nuclei. To generate the Zernike shape features of the nucleus, we identified the circle with the smallest diameter covering the tumor nucleus, assigned a value of 1 to all pixels within the tumor nucleus and 0 to the background, and decomposed the resulting binary image into Zernike polynomials. The resulting coefficients were then used as features.[29] The findings highlight the importance of considering subtle nuclear shape patterns in predicting patient prognosis.

In rectal cancer, the strength of the *in situ* adaptive immune reaction strongly correlates with the survival outcome.[30,31] The scoring system known as IS is utilized to evaluate the densities of CD3+ and CD8+ T cells at both the tumor region and invasive margin.[21] The IS has potential as a valuable prognostic indicator for rectal cancer patients who underwent surgical treatment. El Sissy et al.[20] established that IS_B carried out on biopsy specimens, the only sample material available before treatment, is an adaptation of the standardized IS carried out on surgical specimens. Deriving IS_B before nCRT offers the advantage of assessing the initial immune response in the tumor and its possible impact on the treatment response and prognosis. Similarly, our study demonstrated that IS_B could independently predict DM-free survival in LARC patients. Patients with low IS_B had a remarkably higher risk of DM than those with intermediate and high IS_B. In addition, we compared the distribution of the risk scores of radiomics and pathomics signatures among patients with different groups of IS_B and confirmed the intimate association between radiomics or pathomics and immune infiltrating status.

There are several limitations in this study. Firstly, the study is retrospective in nature, and data collection was limited to a single medical center. It is imperative for future studies to encompass prospective research conducted at multiple centers. Secondly, the manual delineation of the VOIs added a certain degree of human intervention to the predictive model. To improve model reliability, future investigations may explore developing an entirely automated tumor segmentation process. Thirdly, there could be potential issues related to tissue heterogeneity and sampling bias as pathomics features and IS_B were obtained from biopsy specimens.

CONCLUSIONS

This study explored a nomogram that utilized macro- and microscopic tumor characteristics at baseline, including radiomics, pathomics, and IS_B, to predict DM before treatment for patients with LARC. The nomogram is an effective tool to identify high-risk patients with DM and develop personalized treatment.

ACKNOWLEDGEMENTS

The authors thank Editage (https://www.editage.cn) for its linguistic assistance during the preparation of the manuscript.

FUNDING

This work was supported by Capital's Funds for Health Improvement and Research (CFH) [grant number 2022-2-4024]; the National Natural Science Foundation of China [grant number 81971589]; CAMS Innovation Fund for Medical Sciences (CIFMS) [grant number 2021-I2M-C&T-A-017]; and CAMS Clinical and Translational Medicine Research [grant number 2022-I2M-C&T-B-073].

DISCLOSURE

The authors have declared no conflicts of interest.

REFERENCES

1. Sauer R, Becker H, Hohenberger W, et al. Preoperative versus postoperative chemoradiotherapy for rectal cancer. *N Engl J Med*. 2004;351(17):1731-1740.
2. Bosset JF, Collette L, Calais G, et al. Chemotherapy with preoperative radiotherapy in rectal cancer. *N Engl J Med*. 2006;355(11):1114-1123.
3. van Gijn W, Marijnen CA, Nagtegaal ID, et al. Preoperative radiotherapy combined with total mesorectal excision for resectable rectal cancer: 12-year follow-up of the multicentre, randomised controlled TME trial. *Lancet Oncol*. 2011;12(6):575-582.
4. Fokas E, Liersch T, Fietkau R, et al. Tumor regression grading after preoperative chemoradiotherapy for locally advanced rectal carcinoma revisited: updated results of the CAO/ARO/AIO-94 trial. *J Clin Oncol*. 2014;32(15):1554-1562.
5. Bosset JF, Calais G, Mineur L, et al. Fluorouracil-based adjuvant chemotherapy after preoperative chemoradiotherapy in rectal cancer:

long-term results of the EORTC 22921 randomised study. *Lancet Oncol*. 2014;15(2):184-190.
6. Yoo RN, Kim HJ. Total neoadjuvant therapy in locally advanced rectal cancer: role of systemic chemotherapy. *Ann Gastroenterol Surg*. 2019;3(4):356-367.
7. Tamburini E, Tassinari D, Ramundo M, et al. Adjuvant chemotherapy after neoadjuvant chemo-radiotherapy and surgery in locally advanced rectal cancer. A systematic review of literature with a meta-analysis of randomized clinical trials. *Crit Rev Oncol Hematol*. 2022;172:103627.
8. Lambin P, Rios-Velazquez E, Leijenaar R, et al. Radiomics: extracting more information from medical images using advanced feature analysis. *Eur J Cancer*. 2012;48(4):441-446.
9. Liu Z, Meng X, Zhang H, et al. Predicting distant metastasis and chemotherapy benefit in locally advanced rectal cancer. *Nat Commun*. 2020;11(1):4308.
10. Liu X, Zhang D, Liu Z, et al. Deep learning radiomics-based prediction of distant metastasis in patients with locally advanced rectal cancer after neoadjuvant chemoradiotherapy: a multicentre study. *EBioMedicine*. 2021;69:103442.
11. Bhargava R, Madabhushi A. Emerging themes in image informatics and molecular analysis for digital pathology. *Ann Rev Biomed Eng*. 2016;18:387-412.
12. Saltz J, Gupta R, Hou L, et al. Spatial organization and molecular correlation of tumor-infiltrating lymphocytes using deep learning on pathology images. *Cell Rep*. 2018;23(1):181-193.e187.
13. Feng L, Liu Z, Li C, et al. Development and validation of a radiopathomics model to predict pathological complete response to neoadjuvant chemoradiotherapy in locally advanced rectal cancer: a multicentre observational study. *Lancet Digit Health*. 2022;4(1):e8-e17.
14. Wan L, Sun Z, Peng W, et al. Selecting candidates for organ-preserving strategies after neoadjuvant chemoradiotherapy for rectal cancer: development and validation of a model integrating MRI radiomics and pathomics. *J Magn Reson Imaging*. 2022;56(4):1130-1142.
15. Fridman WH, Pagès F, Sautès-Fridman C, Galon J. The immune contexture in human tumours: impact on clinical outcome. *Nat Rev Cancer*. 2012;12(4):298-306.
16. Galon J, Mlecnik B, Bindea G, et al. Towards the introduction of the 'Immunoscore' in the classification of malignant tumours. *J Pathol*. 2014;232(2):199-209.
17. Yasuda K, Nirei T, Sunami E, Nagawa H, Kitayama J. Density of CD4(+) and CD8(+) T lymphocytes in biopsy samples can be a predictor of pathological response to chemoradiotherapy (CRT) for rectal cancer. *Radiat Oncol*. 2011;6:49.
18. Anitei MG, Zeitoun G, Mlecnik B, et al. Prognostic and predictive values of the immunoscore in patients with rectal cancer. *Clin Cancer Res*. 2014;20(7):1891-1899.
19. Shinto E, Hase K, Hashiguchi Y, et al. CD8+ and FOXP3+ tumor-infiltrating T cells before and after chemoradiotherapy for rectal cancer. *Ann Surg Oncol*. 2014;21(suppl 3):S414-S421.
20. El Sissy C, Kirilovsky A, Van den Eynde M, et al. A diagnostic biopsy-adapted immunoscore predicts response to neoadjuvant treatment and selects patients with rectal cancer eligible for a watch-and-wait strategy. *Clin Cancer Res*. 2020;26(19):5198-5207.
21. Pagès F, Mlecnik B, Marliot F, et al. International validation of the consensus Immunoscore for the classification of colon cancer: a prognostic and accuracy study. *Lancet*. 2018;391(10135):2128-2139.
22. Saltz J, Almeida J, Gao Y, et al. Towards generation, management, and exploration of combined radiomics and pathomics datasets for cancer research. *AMIA Jt Summits Transl Sci Proc*. 2017;2017:85-94.
23. Jiang Y, Chen C, Xie J, et al. Radiomics signature of computed tomography imaging for prediction of survival and chemotherapeutic benefits in gastric cancer. *EBioMedicine*. 2018;36:171-182.
24. Liu Z, Zhang XY, Shi YJ, et al. Radiomics analysis for evaluation of pathological complete response to neoadjuvant chemoradiotherapy in locally advanced rectal cancer. *Clin Cancer Res*. 2017;23(23):7253-7262.
25. Horvat N, Veeraraghavan H, Khan M, et al. MR imaging of rectal cancer: radiomics analysis to assess treatment response after neoadjuvant therapy. *Radiology*. 2018;287(3):833-843.
26. Shin J, Seo N, Baek SE, et al. MRI radiomics model predicts pathologic complete response of rectal cancer following chemoradiotherapy. *Radiology*. 2022;303(2):351-358.
27. Chen D, Fu M, Chi L, et al. Prognostic and predictive value of a pathomics signature in gastric cancer. *Nat Commun*. 2022;13(1):6903.
28. Yu KH, Zhang C, Berry GJ, et al. Predicting non-small cell lung cancer prognosis by fully automated microscopic pathology image features. *Nat Commun*. 2016;7:12474.
29. Boland MV, Markey MK, Murphy RF. Automated recognition of patterns characteristic of subcellular structures in fluorescence microscopy images. *Cytometry*. 1998;33(3):366-375.
30. Mlecnik B, Tosolini M, Kirilovsky A, et al. Histopathologic-based prognostic factors of colorectal cancers are associated with the state of the local immune reaction. *J Clin Oncol*. 2011;29(6):610-618.
31. Koelzer VH, Dawson H, Andersson E, et al. Active immunosurveillance in the tumor microenvironment of colorectal cancer is associated with low frequency tumor budding and improved outcome. *Transl Res*. 2015;166(2):207-217.